

# Nitrogen localized states in dilute $\text{GaAs}_{1-x}\text{N}_x$ alloys: effect of N interstitial complexes on the electronic properties, from first principles

J. D. Querales-Flores,<sup>1,2,3,\*</sup> C. I. Ventura,<sup>2,4</sup> and J. D. Fuhr<sup>2,3</sup>

<sup>1</sup>*Tyndall National Institute, Lee Maltings, Dyke Parade, Cork (T12 R5CP), Ireland*

<sup>2</sup>*Centro Atómico Bariloche-CNEA and CONICET, Av. Bustillo Km. 9.5, 8400-Bariloche, Argentina*

<sup>3</sup>*Instituto Balseiro, Univ. Nac. de Cuyo and CNEA, 8400-Bariloche, Argentina*

<sup>4</sup>*Univ. Nac. de Río Negro, 8400-Bariloche, Argentina*

(Dated: 14 December 2024)

Several approaches have been used to investigate the impact of Nitrogen (N) on the electronic structure of  $\text{GaAs}_{1-x}\text{N}_x$  alloys, however, there is no agreement between theory and experiments about the importance of the different N interstitial defects in these alloys, and their nature is still unknown. Here we analyze the impact of five different N defects on the electronic structure of  $\text{GaAs}_{1-x}\text{N}_x$  alloys, using density-functional methods: we calculate electronic states, formation energies and charge transition levels. The studied defects include  $\text{N}_{\text{As}}$ ,  $\text{As}_{\text{Ga}}$ ,  $\text{As}_{\text{Ga}}\text{-N}_{\text{As}}$  substitutional defects, and  $(\text{N-N})_{\text{As}}$ ,  $(\text{N-As})_{\text{As}}$  split-interstitial complex defects. Our calculated defect formation energies agree with those reported by S.B. Zhang et al. [Phys. Rev. Lett. 86, 1789 (2001)], who predicted these defects. Among the interstitial defects, we found that  $(\text{N-As})_{\text{As}}$  emerges as the lowest energy configuration in comparison with  $(\text{N-N})_{\text{As}}$ , agreeing with recent experiments [T. Jen, et al., Appl. Phys. Lett. 107, 221904 (2015)]. We also calculated the levels induced in the electronic structure due to each of these defects: defect states may occur as deep levels in the gap, shallow levels close to the band edges, and as levels between bulk states. We find that the largest changes in the band structure are produced by an isolated N atom in GaAs, which is resonant with the conduction band, exhibiting a strong hybridization between N and GaAs states. Deeper levels in the bandgap are obtained with  $(\text{N-N})_{\text{As}}$  split-interstitial defects. Our results confirm the formation of highly localized states around the N sites, which is convenient for applications.

## I. INTRODUCTION

Defects, whether intentional or not, have a dominant impact in both electrical and optical properties of semiconductor alloys.<sup>1</sup> The rich variety of defects along with their technological importance guarantee interest to their computational research. III-N-V semiconductors, in particular GaAsN alloys, are promising for a wide range of applications including the next-generation of high-efficiency multijunction solar cells, high-performance electronic devices and long-wavelength light emitters and detectors, because these materials can be lattice matched to substrates such as GaAs, Ge and Si, with a range of direct gaps that are complementary to those of other III-V semiconductors.<sup>1-5</sup>

Experimental and theoretical works have suggested that the majority of Nitrogen atoms incorporated to GaAs could be expected to go to isoelectronic substitutional As sites.<sup>6,7</sup> However, Zhang and Wei<sup>6</sup> suggested that a significant fraction of N atoms incorporate non-substitutionally as N-N split interstitials,  $(\text{N-N})_{\text{As}}$ , or  $(\text{N-As})_{\text{As}}$  split interstitials.

---

\*<sup>1</sup>jose.querales@tyndall.ie

Direct measurements of the fraction of N incorporated interstitially in GaAs via nuclear reaction analysis (NRA) have been reported by several groups.<sup>8–12</sup> More recently, Jen et al.<sup>12</sup> reported a comparison between Rutherford backscattering spectroscopy and NRA with Monte Carlo-Molecular Dynamics simulations, in order to distinguish  $(\text{N-N})_{\text{As}}$ ,  $(\text{N-As})_{\text{As}}$  and  $(\text{As}_{\text{Ga}}\text{-N}_{\text{As}})$  interstitial complexes in GaAsN alloys. The results suggested that  $(\text{N-As})_{\text{As}}$  is the dominant interstitial complex in dilute GaAsN, in contrast to previous electronic structure calculations, based on density functional theory (DFT), which predicted  $(\text{N-N})_{\text{As}}$  to be the most energetically favorable configuration.<sup>7,13</sup> In 2017, Occena et al.<sup>14</sup> examined the influence of Bismuth and Nitrogen fluxes on N and Bi incorporation during molecular beam epitaxy of  $\text{GaAs}_{1-x-y}\text{N}_x\text{Bi}_y$  alloys, and observed an enhancement in total N incorporation via the formation of additional  $(\text{N-As})_{\text{As}}$ .

The relationship between interstitial N incorporation and the electronic properties of GaAsN has not been reported yet. Nevertheless, several theoretical approaches have been used in order to investigate the impact of N on the electronic structure of  $\text{GaAs}_{1-x}\text{N}_x$  alloys. For instance, first-principles,<sup>7,13,15,16</sup> empirical pseudopotential,<sup>17,18</sup> and  $sp^3s^*$  tight-binding<sup>19–21</sup> calculations of supercells have been performed, giving valuable insight on the microscopic mechanisms of formation of band-edge states in  $\text{GaAs}_{1-x}\text{N}_x$ . The band structure of  $\text{GaAs}_{1-x}\text{N}_x$  substitutional alloys was studied in the framework of DFT within the hybrid functional scheme (HSE06),<sup>22</sup> and it was found that the trends in the bandgap reduction in these alloys result mainly from the positions of the N-induced states with respect to the bottom of the bulk conduction bands. Ref. 23 demonstrated the accuracy of HSE06 hybrid functional for computing the band offsets of semiconductor alloy heterostructures, including GaAs. The formation energies and transition levels of a set of interstitial-type defects of N in GaAs have been determined by DFT calculations, in local density approximation (LDA)<sup>13</sup> and generalized gradient approximation (GGA).<sup>7</sup> Nevertheless, for N-N split interstitial defects, differences were observed between the bandgap transition levels calculated with LDA and GGA approximations.<sup>7,13</sup>

It is known that point-defect formation energies calculated within the framework of density functional theory often depend on the choice of the exchange and correlation ( $xc$ ) functional. Regarding that, Freysoldt, Lange and Neugebauer<sup>24</sup> showed that variations between the LDA, GGA, and hybrid functionals emerge from differences in the position of the bulk valence-band maximum, as well as in the reference energies for the chemical potential obtained with distinct  $xc$  functionals. Freysoldt et al.<sup>24</sup> used a band-alignment strategy, based on aligning a benchmark defect level between GGA and hybrid functional calculations; they also included changes to reference energies for chemical potentials between functionals.

In this work, we determine formation energies and charge transition levels for a large set of Nitrogen defects in GaAs using a supercell approach for defects calculations in GGA approximation and hybrid functionals calculations for the reference energies for the chemical potential, adopting the framework recently proposed in Ref.24. In particular, we investigate the case of single-atom substitutional defects  $\text{N}_{\text{As}}$  and  $\text{As}_{\text{Ga}}$ . We also consider complex defects such as  $\text{As}_{\text{Ga}}\text{-N}_{\text{As}}$ , in which the  $\text{N}_{\text{As}}$  defect binds to one  $\text{As}_{\text{Ga}}$  antisite, and split interstitials  $\text{N-N}_{\text{As}}$  and  $\text{N-As}_{\text{As}}$ , in which a dimer of N-N or N-As is located in an As site. Our results suggest that  $(\text{N-As})_{\text{As}}$  is the dominant split interstitial in dilute GaAsN, in agreement with recent experimental results.<sup>12,14</sup> We also calculated the induced levels in the electronic structure due to each of these defects. Depending on the defect, these states occur as deep levels in the band gap, as shallow levels very close to the band edges, as well as levels in-between the bulk states. We find that the most prominent of these levels is due to an isolated Nitrogen atom in GaAs, which is resonant with the conduction band, exhibiting a strong hybridization between Nitrogen and GaAs states. Deeper lines in the energy gap have been found with Nitrogen pairs. These results confirm the formation of highly localized electronic states around the Nitrogen sites, which is favourable for applications.<sup>5,25</sup>

This paper is organized as follows. In Sec. II, we describe our theoretical approach based on DFT calculations. In particular, we discuss the method we adopted to calculate the defect formation energies by combining GGA and hybrid functionals calculations. The results of our calculations are given in Sec. III, where they are compared to previous theoretical and experimental results. In Sec. IV, the conclusions are summarized.

## II. THEORETICAL APPROACH

The most relevant thermodynamic quantity characterizing a point defect  $X$  in charge state  $q$  is its formation energy, as comprehensively reviewed by Van de Walle, Neugebauer et al. in Refs. 26,27, given by:

$$E_f(X^q) = E_t[X^q] - E_t[Bulk] - \sum_i n_i \mu_i + q[\mu_e + \Delta V] \quad (1)$$

which depends on the chemical potentials  $\mu_i$  of atoms that have been added ( $n_i > 0$ ) or removed ( $n_i < 0$ ) and the chemical potential for electrons  $\mu_e = E_F + E_{VBM}$ , being  $E_F$  and  $E_{VBM}$  the Fermi level and the valence band maximum respectively.  $E_t[X^q]$  and  $E_t[GaAs]$  are the calculated total energies of the defect  $X$  (in charge state  $q$ ) and bulk respectively. The chemical potentials  $\mu_i$  of  $n_i$  added or removed atoms allow us to take into account the growth conditions.  $\Delta V$  corresponds to a correction for the finite size of charged supercells, in order to align the potentials of the two supercells.<sup>13</sup>

We have determined the formation energies and transition levels of Nitrogen defects in GaAs, with spin-polarized DFT total energy calculations. All defect configurations are obtained through full structural relaxation carried out within a DFT framework in which the exchange-correlation energy is described through the semilocal approximation proposed by Perdew, Burke, and Ernzerhof.<sup>28,29</sup> To obtain the chemical potential of atoms,  $\mu_i$  in Eq.1, we performed calculations using the screened hybrid functional of Heyd, Scuseria, and Ernzerhof (HSE).<sup>30,31</sup> We used the VASP (Vienna Ab-initio Simulation Package) code<sup>32</sup> with the projector augmented wave (PAW). We use a plane-basis set defined by a kinetic energy cutoff of 400 eV and the Gallium  $3d$  states were treated as valence states. We performed calculations using 64 and 65-atoms supercells with a  $3 \times 3 \times 3$   $k$ -point set generated using the Monkhorst-Pack method. We fully relax the unit cell to obtain the lattice constants for GaAs of 5.7497 Å, consistent with earlier reports<sup>33</sup>. The atomic positions are relaxed until the Hellmann-Feynman force acting on each atom is reduced down to less than 1.0 meV/Å. The unfolding of the supercell bandstructure has been performed using the BandUP code<sup>34,35</sup>.

## III. RESULTS AND DISCUSSION

Here, we will present structural and electronic structure results obtained using our approach described in Sec.II, in four subsections. In Sec. III A, we will discuss and compare our results for the structural properties for the N defects studied, with recent theoretical values, when available. In Sec. III B, we show our results for the total and projected densities of states, in order to identify the N-induced electron states around the gap of GaAs. In Sec.III C we analyze the formation energies for charged defects, for all studied N configurations as a function of Fermi energy. In Sec.III D, we will describe the unfolded band structure for each N defect in connection with the results first presented in Sec.III B.

### A. Structure of the studied defects

Figure 1 shows the structure of the As atoms in GaAs (Fig. 1(a)) along with the five complex defects studied in this work (Figs. 1(b)-(e)). When a Nitrogen atom is incorporated in an As substitutional lattice site, the following bonds are formed with respective bond-lengths: 2.1119 Å for N-Ga, and 2.4902 Å for As-Ga. We found that N incorporates in the split interstitial (N-N), in which two N atoms share a substitutional lattice site with a strong bond between them: 1.3349 Å is the N-N bond-length and 2.0220 Å the N-Ga one. The N-N bond-length results are consistent with previous LDA studies: i.e. 1.34 Å<sup>13</sup>, and 1.33 Å<sup>7</sup>; while the value obtained for the N-Ga bond-length is slightly larger than 1.95 Å reported in Ref.13.

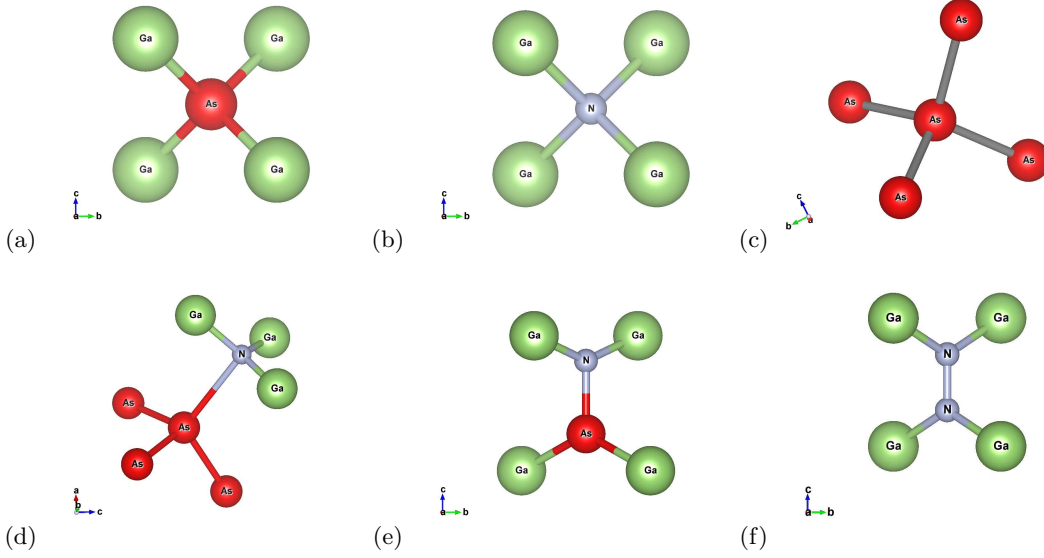


FIG. 1. Configurations of native defects in  $\text{GaAs}_{1-x}\text{N}_x$ . (a) Crystalline GaAs, (b) single Nitrogen atom located in an Arsenic site,  $\text{N}_{\text{As}}$ , (c) single Arsenic atom located in a Gallium site,  $\text{As}_{\text{Ga}}$ , (d)  $\text{N}_{\text{As}}$  defect binds to one  $\text{As}_{\text{Ga}}$  antisite,  $\text{As}_{\text{Ga}}\text{-N}_{\text{As}}$ , (e) Nitrogen-Arsenic pair in an Arsenic site,  $(\text{N-As})_{\text{As}}$  and (f) Nitrogen dimer in an Arsenic site,  $(\text{N-N})_{\text{As}}$ . The figures were generated using VESTA software.<sup>36</sup>

When N incorporates in the other split interstitial configuration, in which a dimer with N-As atoms occupies a substitutional lattice site and we find 1.7998 Å for N-As bond-length (LDA: 1.79 Å<sup>13</sup>), 2.4351 Å for As-Ga bonds (LDA: 2.38 Å<sup>13</sup>) and 1.9298 Å for N-Ga bonds (LDA: 1.88 Å<sup>13</sup>). For substitutional  $\text{As}_{\text{Ga}}$ , we find that 2.6085 Å As-As, and 4.0893 Å As-Ga bonds are formed.

## B. Electron density of states

We first calculate the total and projected densities of states of  $\text{GaAs}_{1-x}\text{N}_x$  for the five N defects considered in this study. In order to further understand the defect states in the band gap, in Figure 2 we show the the total density of states and the projected density of states on each defect, including the contribution from the four first neighbours around each defect configuration. Here, the energy axis is referenced with respect the Fermi level of bulk GaAs. From the density of states we can get information about the carrier type induced by each kind of defects. In particular, we find that for the defects  $\text{As}_{\text{Ga}}$ ,  $(\text{N-As})_{\text{As}}$ ,  $(\text{N-N})_{\text{As}}$ ,  $\text{As}_{\text{Ga}}\text{-N}_{\text{As}}$ , localized states can be identified within the bulk GaAs bandgap,  $E_g$ , which is indicated by vertical dotted lines in Fig.2. Notice that DFT(GGA) provides a smaller direct bandgap with respect to the experimentally reported one: using the GGA optimized lattice parameter  $E_g = 0.18\text{eV}$ , which increases to 0.56 eV if the experimental lattice parameter is used in the calculation, while the experimental direct gap is  $\sim 1.52\text{eV}$ <sup>23,37</sup>. Meanwhile, for substitutional  $\text{N}_{\text{As}}$  no localized states can be identified, indicating a strong hybridization between N-states and GaAs states at the edge of the valence and/or conduction bands. The localized character of the  $(\text{N-N})_{\text{As}}$  dimers was suggested from first-principles pseudopotential method studies in Ref. 38.

## C. Thermodynamic transition levels of N defects in $\text{GaAs}_{1-x}\text{N}_x$

According to Eq. 1 the higher the Fermi level is, the more energy is gained by moving the electron from the reservoir into the defect. That is, the formation energy of a negatively

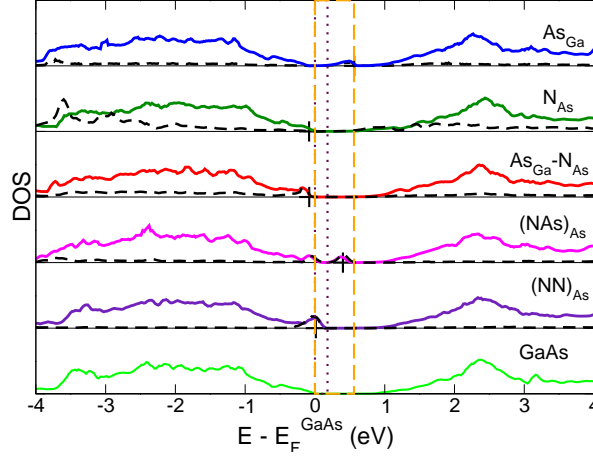


FIG. 2. Total density of states (DOS) for GaAs including the five defect configurations, for comparison the total density of states for bulk GaAs is included. Full lines represent the DOS and dashed lines the projected densities of states on each defect and the contribution from the four first neighbours around each defect. The PDOS corresponding to  $N_{As}$  was multiplied by a factor 10. The small vertical full lines indicate the Fermi level for each defect configuration. Vertical lines along the whole figure indicate the band gap for pure GaAs: dotted lines (obtained by using the optimized lattice parameter in the DFT calculation) and dashed lines (obtained by using the experimental lattice parameter in the DFT calculation).

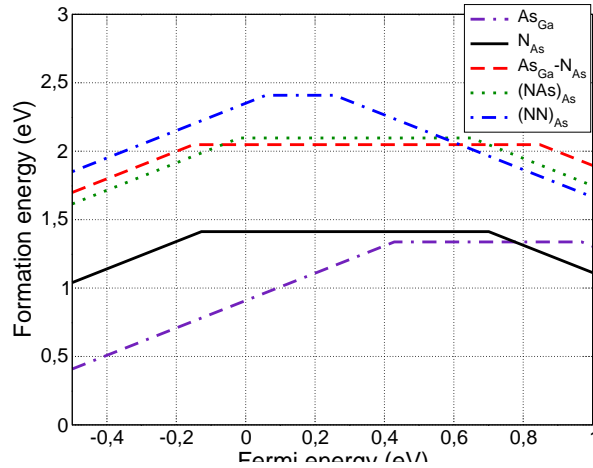


FIG. 3. Formation energies vs. Fermi level for substitutional, interstitial, and antisite defects in  $\text{GaAs}_{1-x}\text{N}_x$ , calculated with a GGA and HSE hybrid functionals corrections, as proposed by Freysoldt et al. in Ref. 24. All sets of formation energies include finite-size corrections (see last term in Eq. 1). The Fermi-level range is extended beyond the band maxima. In all cases, Ga-rich conditions are chosen. The lattice constant was taken as the DFT-GGA one, mentioned in Sec.II.

charged defect gets lower at higher values of the Fermi level, and viceversa for the positively charged defects. If the defect has the lowest formation energy in the negative charge state, then a neutral defect would like to receive an electron from the electron reservoir, so that it behaves like an acceptor. In a similar way, if a neutral defect likes to donate an electron to the electron reservoir, it becomes positively charged and this can be related with a donor. When the formation energies of all the possible charge states are calculated, the charge state yielding the lowest formation energy depends on the Fermi level. Consequently, there

TABLE I. Charge transition levels ( $\epsilon_{q/q'}$ ), Fermi energy for neutral defects ( $E_F^0$ ) and formation energies ( $E_f$ ) calculated at the PBE level, and including hybrid functional corrections for electron and chemical reservoirs and Ga 3d states in the valence band, for the most relevant defects. For comparison, we also show corresponding formation energies calculated in Refs.7, 13, and 33.  $E_F^0$  for GaAs: 2.717 eV.

Defect	$E_F^0$ (eV)	$E_f$ (eV)	$\epsilon_{+1/0}$ (eV)	$\epsilon_{0/-1}$ (eV)
As <sub>Ga</sub>	3.280	1.337 (1.33 <sup>33</sup> )	0.428	0.969
N <sub>As</sub>	2.633	1.406 (1.087 <sup>7</sup> )	-0.128	0.7
As <sub>Ga</sub> -N <sub>As</sub>	2.635	2.048	-0.151	0.848
(N-As) <sub>As</sub>	3.118	2.178 (2 <sup>13</sup> )	-0.018	0.651 (0.29 <sup>13</sup> )
(N-N) <sub>As</sub>	2.730	2.462 (2.754 <sup>7</sup> )	0.058 (0.2 <sup>7</sup> )	0.256 (0.12 <sup>13</sup> , 0.3 <sup>7</sup> )

will be a value of  $E_F$  where the formation energy is the same for two charge states, which is usually denoted as ionization level, hereafter denoted as  $\epsilon(q_1/q_2)$ . This level is the same as the energy required to promote an electron from the valence band into the defect for acceptor levels or demoting an electron from the defect to the valence band for donor levels. The atomic structures of the defects in charge states  $q_1$  and  $q_2$  are probably different. If the atomic relaxation occurs during the ionization process, it is called thermodynamic transition. If not, it is called an optical transition. Formation energies for thermodynamic transitions of native defects in GaAs<sub>1-x</sub>N<sub>x</sub> calculated with GGA (PBE) and HSE are presented in Fig. 3. Ga-rich conditions ( $\mu_{Ga} = \mu_{Ga,bulk}$ ) in Eq. 1 have been chosen. In our calculation, for each charged defect configuration a fully structural relaxation was done.

Figure 3 shows the calculated formation energies for all studied defects as a function of Fermi energy. In the following we describe the main results exhibited in Fig.3:

*N-N split interstitials*: N gives rise to two transition levels within the band gap of GaAs<sub>1-x</sub>N<sub>x</sub>. Concretely, the transition from the neutral to +1 charge state (0/+1) happens when the Fermi energy is 0.058 eV above the valence band maximum, while the transition from the neutral to -1 charge state (0/-1) occurs at a Fermi energy equal to 0.256 eV. This defect was found to be stable in positively charged states when the Fermi level is in the lower part of the band gap, stable in the neutrally charged state for a limited number of values of the Fermi level in the gap, and becoming negatively charged at higher Fermi levels.

*N-As split interstitials*: Only one transition level within the band gap of GaAs<sub>1-x</sub>N<sub>x</sub> is found, from neutral to -1 charge state (0/-1) at the Fermi energy 0.651 eV. For most Fermi energy values the interstitial defect with the lowest energy is (N-As)<sub>As</sub>.

*N substitutional*: We find one transition level in the band gap for the substitutional N<sub>As</sub> and As<sub>Ga</sub>-N<sub>As</sub> antisite defects: the transition (0/-1) happens for the N<sub>As</sub> and As<sub>Ga</sub>-N<sub>As</sub> defects at Fermi energies of 0.7 and 0.848 eV above VBM, respectively.

*As<sub>Ga</sub> substitutional*: we find two transition levels in the band gap: (+1/0) happens defect at Fermi energy 0.428 and (0/-1) at 0.969 eV above VBM, respectively. The occupation of the Ga site by As leads to insignificant lattice distortions, involving the formation of defects with the lowest formation energy.

The calculated charge transition levels, Fermi energy for neutral defects and formation energies, are listed in Table I together with the results of previous first-principles calculations, for comparison.

#### D. Unfolding of the supercell bandstructures

In the next step, to get meaningful information from the massive number of bands of a GaAs with N defects system, we employ the technique of band unfolding by using the recently released BandUP code.<sup>34,35</sup> With this technique we can obtain the unfolding of the bands in the Brillouin zone (BZ) of the large supercell back into the BZ of the primitive unit cell of GaAs. As reference, the unfolded band structure of GaAs close to the bandgap is shown in Fig. 4. Our GGA calculation gives a direct gap of  $\sim 0.4$  eV, which is considerably

underestimated with respect to the experimental results, 1.52 eV at 0 K and 1.43 eV at 300 K.<sup>39</sup>

The unfolded band structure for GaAs with each of the different Nitrogen defects considered in this work, along high-symmetry directions of the primitive cell BZ are shown in Figs. 5, 6, 7, and 8, respectively. As a general result, it can be seen that by introducing N defects in GaAs, some new bands with low Bloch spectral weight appear, mostly close to the bandgap. In the following we will discuss more in detail the effect of each of the N defects on the electronic band structure of GaAs.

In Figure 5, we exhibit the unfolded band structure of GaAs with substitutional  $N_{As}$  defects. We observe that  $N_{As}$  defects mostly affect the conduction band of GaAs (compare with Fig. 4), causing the formation of quasilocalized electron states associated with the substitutional N atoms, which interact strongly with the GaAs conduction band edge. In particular, the lowest energy conduction band is splitted, and a second minimum appears at  $\Gamma$  which possesses very low spectral weight. Our results are in agreement with previous studies by Shan et al.,<sup>40</sup> where a simple physical understanding of the dramatic effect of  $N_{As}$  defects on the bandgap of GaAs was based on the band anticrossing model, and they showed that the reduction of the energy bandgap could be described by an interaction between the conduction band and a higher-lying set of localized N resonant states.<sup>21,41</sup> These results agree with our DOS calculations presented in Fig.2, where localized N-induced states are not identified when N is incorporated substitutionally.

In Figure 6, we exhibit the unfolded band structure of GaAs with  $(N-N)_{As}$  and  $(N-As)_{As}$  complex interstitial defects. As can be seen in the figure, the lowest energy conduction band is less affected by this defect configuration, in contrast to our findings for the substitutional  $N_{As}$  defects discussed above. In agreement with results previously presented in Figure 2,  $N-N_{As}$  induces quite localized states in the top of the GaAs valence band, which can be seen in the band structure as flat lines with very low spectral weight just below the Fermi level.

In Figure 7, we exhibit the unfolded band structure of GaAs with  $As_{Ga}-N_{As}$  defects. We observe that this defect affects both the conduction and valence bands of GaAs, producing

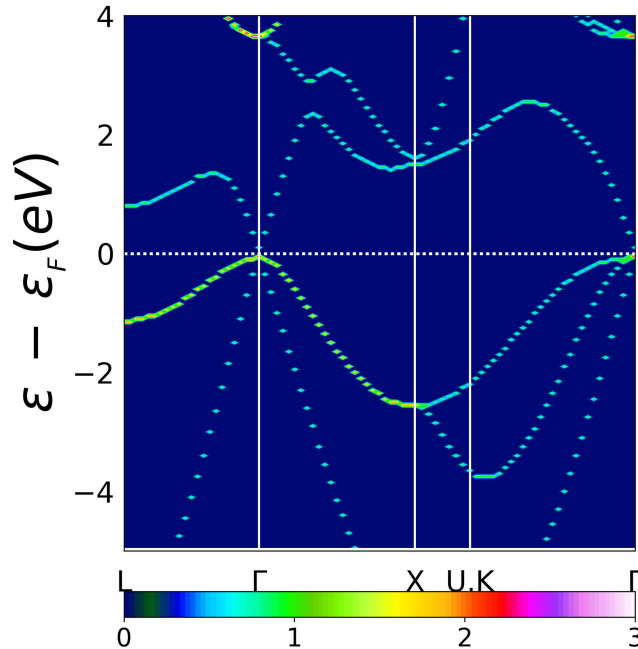


FIG. 4. Effective band structure of a 64 atoms supercell of GaAs, unfolded into a primitive cell of the Brillouin zone using the BandUp code.<sup>34,35</sup>

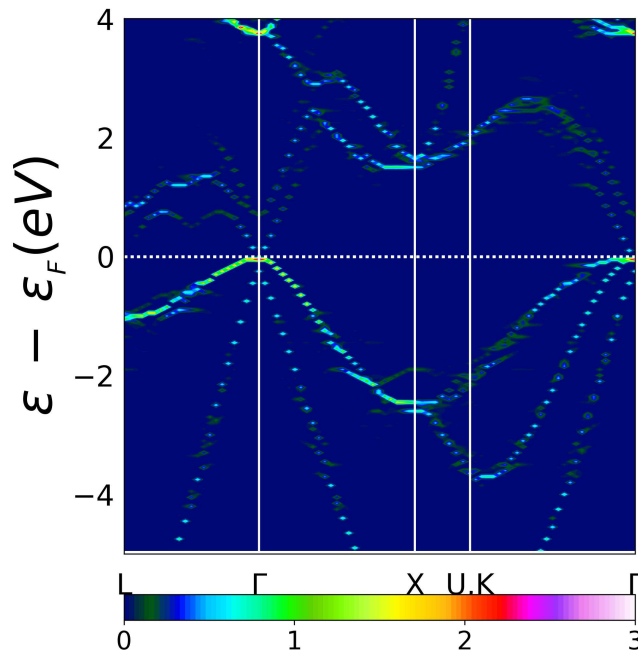


FIG. 5. Unfolded 64 atoms supercell band structure for a  $N_{As}$  defect in GaAs.

firstly a reduction of the direct gap, as for  $N_{As}$ , and secondly the formation of quasilocalized electron states near the top of the GaAs valence bands. The lines appearing very close to the conduction band in Fig.7 can be observed as a sharp peak in the DOS, as shown in Fig.2.

Figure 8 shows the unfolded band structure of GaAs with  $As_{Ga}$  substitutional defects. As can be seen in the figure, the electron states associated with an As atom on a Ga site seem to be quasi-localized in the GaAs gap and close the conduction minimum; the DOS corresponding to this configuration in Fig.2, exhibits a sharp peak exactly below the conduction band. In addition, we found that the  $As_{Ga}$  defect does not affect much the band edges in GaAs, opposite to the effect from the N-related defects previously discussed.

#### IV. SUMMARY AND CONCLUSIONS

In this work, we have presented calculations of the structural and electronic properties of dilute  $GaAs_{1-x}N_x$  alloys using a supercell approach, within the framework of density functional theory and the GGA approximation, using a hybrid functional for the exchange correlation functional. Motivated by the fact that semilocal DFT functionals, like GGA, underestimate the band gap of  $GaAs_{1-x}N_x$  alloys, and that this error affects the position of defect levels within the band gap and the values of formation energies, we adopted the Freysoldt et al.<sup>24</sup> method: i.e., using formation energies and defect levels as calculated with GGA, but interpreting them within a bandgap where the valence band edge has been shifted down, and the conduction-band edge has been shifted up, as obtained from a HSE calculation.

We studied the impact of five different N defects on the electronic structure of GaAsN alloys: we calculate the electronic states, formation energies and charge transition levels. The set of studied defects includes  $N_{As}$ ,  $As_{Ga}$ ,  $As_{Ga}-N_{As}$  substitutional defects, and  $(N-N)_{As}$ ,  $(N-As)_{As}$  split-interstitial complex defects. We find that the formation energy of the neutral  $As_{Ga}$  defect is lower than that of substitutional  $N_{As}$ . Meanwhile, the formation energy of neutral  $(N-N)_{As}$  is higher than for all the other defects, while our results also



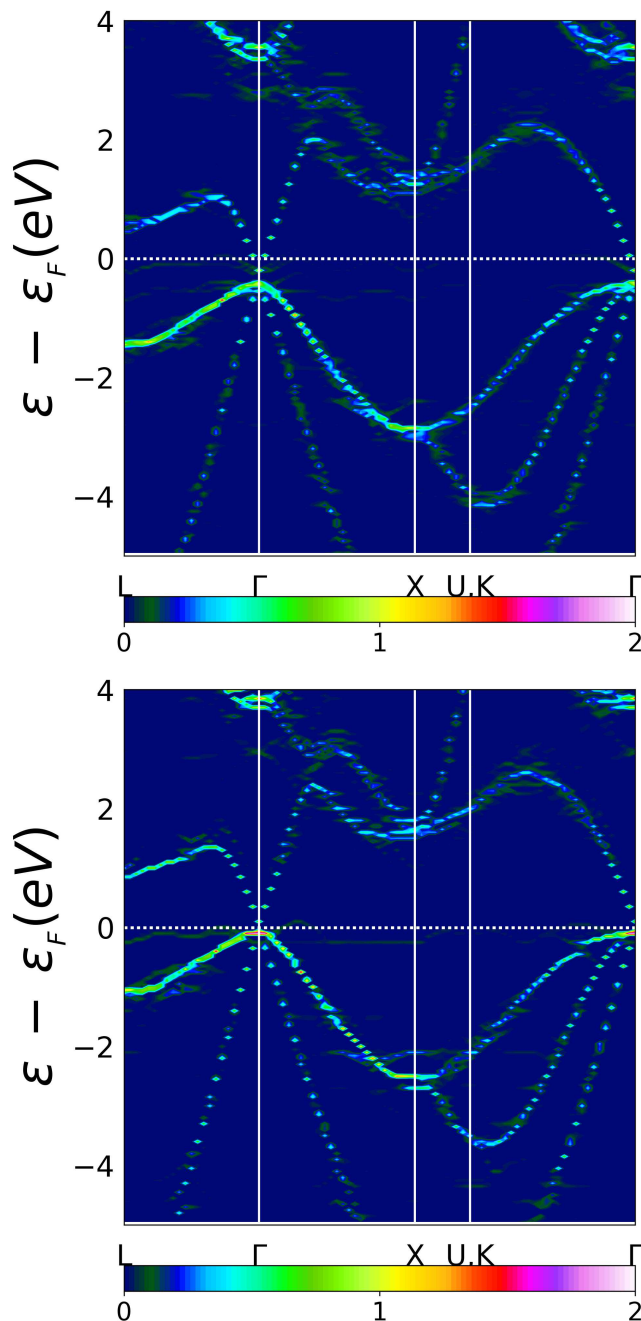


FIG. 6. Unfolded 65 atoms supercell band structure with a: (a)  $(\text{N-As})_{\text{As}}$  interstitial complex defect, and (b)  $(\text{N-N})_{\text{As}}$  interstitial complex defect.

indicate that the  $(\text{N-As})_{\text{As}}$  split interstitial is the dominant interstitial complex defect in the neutral state of dilute GaAsN alloys. These results are in agreement with recent experimental results obtained using Rutherford backscattering spectroscopy and nuclear reaction analysis spectra with Monte Carlo simulations,<sup>12</sup> and other reports for GaAsN and related dilute nitride alloys.<sup>42–47</sup> As a prediction, we find that the antisite  $\text{As}_{\text{Ga}}$  defect is the most favorable one in  $\text{GaAs}_{1-x}\text{N}_x$ . The RBS spectra measured in Ref.12 suggested the possible presence of Ga interstitial and/or As antisite in the  $\text{GaAs}_{1-x}\text{N}_x$  alloys.

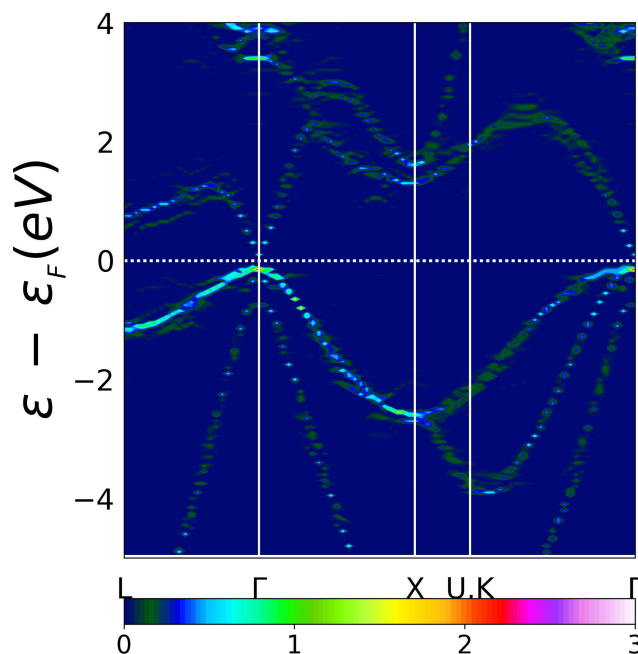


FIG. 7. Unfolded 64 atoms supercell band structure with an  $\text{As}_{\text{Ga}}\text{-N}_{\text{As}}$  substitutional defect.

For the supercell calculations, the band structures were unfolded. Although Nitrogen is isoelectronic with Arsenic, because of the large difference in size and electronegativity between N and As atoms, this causes the formation of quasilocalized electron states associated with the substitution of N atoms, which interact strongly with the GaAs conduction band, and leads to a substantial reduction of the bandgap. We find that the largest changes in the band structure are produced by an isolated N atom in GaAs, which is resonant with the conduction band, exhibiting a strong hybridization between N and GaAs states. Deeper levels in the energy gap, for which the energy required to transfer an electron (or hole) towards the conduction (or valence) band exceeds the characteristic thermal energy ( $k_B T$ ), are obtained with  $(\text{N-N})_{\text{As}}$  split-interstitial defects.

## V. ACKNOWLEDGMENTS

C.I.V. and J.D.F. are Investigadores Científicos of CONICET (Argentina). J.D.Q.-F. thanks CONICET for a postdoctoral fellowship and acknowledges support of PIP 0650 (CONICET) grant. C.I.V. acknowledges support from CONICET - PIP'2015 nr. 11220150100538CO and ANPCyT - PICT'2012 nr. 1069 grants. The authors would like to thank Dr. Paulo V. C. Medeiros and his co-workers for their BandUP code.

<sup>1</sup>J. F. Geisz and D. J. Friedman, *Semiconductor Science and Technology* **17**, 769 (2002), URL <http://stacks.iop.org/0268-1242/17/i=8/a=305>.

<sup>2</sup>M. Fischer, D. Gollub, and A. Forchel, *Japanese Journal of Applied Physics* **41**, 1162 (2002), URL <http://stacks.iop.org/1347-4065/41/i=2S/a=1162>.

<sup>3</sup>J. S. H. Jr, *Semiconductor Science and Technology* **17**, 880 (2002).

<sup>4</sup>S. R. Kurtz, A. A. Allerman, E. D. Jones, J. M. Gee, J. J. Banas, and B. E. Hammons, *Applied Physics Letters* **74**, 729 (1999), <http://dx.doi.org/10.1063/1.123105>, URL <http://dx.doi.org/10.1063/1.123105>.

<sup>5</sup>E. P. O'Reilly, A. Lindsay, P. J. Klar, A. Polimeni, and M. Capizzi, *Semiconductor Science and Technology* **24**, 033001 (2009), URL <http://stacks.iop.org/0268-1242/24/i=3/a=033001>.

<sup>6</sup>S. B. Zhang and S.-H. Wei, *Phys. Rev. Lett.* **86**, 1789 (2001).

<sup>7</sup>P. Carrier, S.-H. Wei, S. B. Zhang, and S. Kurtz, *Phys. Rev. B* **71**, 165212 (2005).

<sup>8</sup>J.-N. Beaudry, R. A. Masut, P. Desjardins, P. Wei, M. Chicoine, G. Bentoumi, R. Leonelli, F. Schietekatte, and S. Guillon, *J. of Vacuum Science & Technology A: Vacuum, Surfaces, and Films* **22**, 771

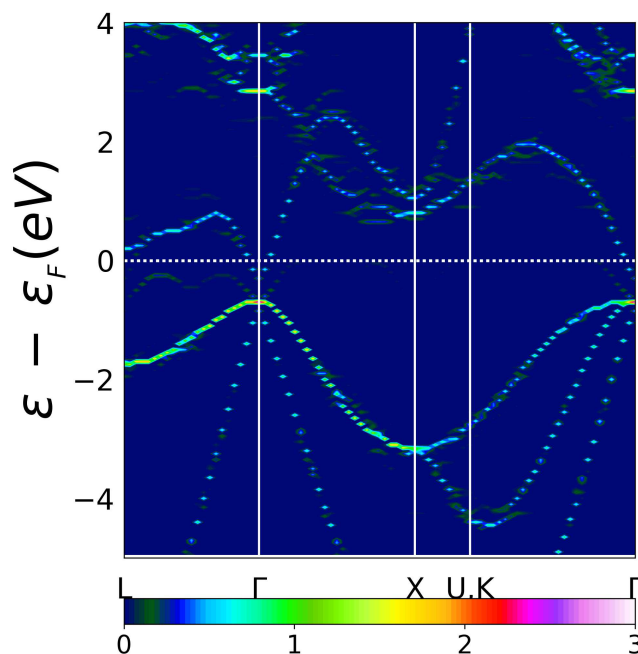


FIG. 8. Unfolded 64 atoms supercell band structure with an  $\text{As}_{\text{Ga}}$  substitutional defect.

- (2004), <http://avs.scitation.org/doi/pdf/10.1116/1.1689296>, URL <http://avs.scitation.org/doi/abs/10.1116/1.1689296>.
- <sup>9</sup>M. Reason, H. A. McKay, W. Ye, S. Hanson, R. S. Goldman, and V. Rotberg, *Applied Physics Letters* **85**, 1692 (2004), <http://dx.doi.org/10.1063/1.1789237>, URL <http://dx.doi.org/10.1063/1.1789237>.
- <sup>10</sup>T. Ahlgren, E. Vainonen-Ahlgren, J. Likonen, W. Li, and M. Pessa, *Applied Physics Letters* **80**, 2314 (2002), <http://dx.doi.org/10.1063/1.1465522>, URL <http://dx.doi.org/10.1063/1.1465522>.
- <sup>11</sup>S. G. Spruytte, C. W. Coldren, J. S. Harris, W. Wampler, P. Krispin, K. Ploog, and M. C. Larson, *Journal of Applied Physics* **89**, 4401 (2001), <http://dx.doi.org/10.1063/1.1352675>, URL <http://dx.doi.org/10.1063/1.1352675>.
- <sup>12</sup>T. Jen, G. Vardar, Y. Q. Wang, and R. S. Goldman, *Applied Physics Letters* **107**, 221904 (2015).
- <sup>13</sup>K. Laaksonen, H.-P. Komsa, T. T. Rantala, and R. M. Nieminen, *Journal of Physics: Condensed Matter* **20**, 235231 (2008).
- <sup>14</sup>J. Occena, T. Jen, E. E. Rizzi, T. M. Johnson, J. Horwath, Y. Q. Wang, and R. S. Goldman, *Applied Physics Letters* **110**, 242102 (2017), <https://doi.org/10.1063/1.4984227>, URL <https://doi.org/10.1063/1.4984227>.
- <sup>15</sup>L.-W. Wang, *Applied Physics Letters* **78**, 1565 (2001), <http://dx.doi.org/10.1063/1.1354162>, URL <http://dx.doi.org/10.1063/1.1354162>.
- <sup>16</sup>B. K. Agrawal, S. Agrawal, P. S. Yadav, and S. Kumar, *Journal of Physics: Condensed Matter* **9**, 1763 (1997), URL <http://stacks.iop.org/0953-8984/9/i=8/a=008>.
- <sup>17</sup>T. Mattila, S.-H. Wei, and A. Zunger, *Phys. Rev. B* **60**, R11245 (1999), URL <http://link.aps.org/doi/10.1103/PhysRevB.60.R11245>.
- <sup>18</sup>P. R. C. Kent and A. Zunger, *Phys. Rev. B* **64**, 115208 (2001), URL <http://link.aps.org/doi/10.1103/PhysRevB.64.115208>.
- <sup>19</sup>M. Gladysiewicz, R. Kudrawiec, J. M. Miloszewski, P. Weetman, J. Misiewicz, and M. S. Wartak, *Journal of Applied Physics* **113**, 063514 (2013), <https://doi.org/10.1063/1.4790568>, URL <https://doi.org/10.1063/1.4790568>.
- <sup>20</sup>A. Lindsay and E. O'Reilly, *Solid State Communications* **112**, 443 (1999), ISSN 0038-1098, URL <http://www.sciencedirect.com/science/article/pii/S0038109899003610>.
- <sup>21</sup>A. Lindsay and E. O'Reilly, *Solid State Communications* **118**, 313 (2001), ISSN 0038-1098, URL <http://www.sciencedirect.com/science/article/pii/S0038109801000643>.
- <sup>22</sup>V. Virkkala, V. Havu, F. Tuomisto, and M. J. Puska, *Phys. Rev. B* **85**, 085134 (2012), URL <http://link.aps.org/doi/10.1103/PhysRevB.85.085134>.
- <sup>23</sup>A. Wadehra, J. W. Nicklas, and J. W. Wilkins, *Applied Physics Letters* **97**, 092119 (2010), <https://doi.org/10.1063/1.3487776>, URL <https://doi.org/10.1063/1.3487776>.
- <sup>24</sup>C. Freysoldt, B. Lange, J. Neugebauer, Q. Yan, J. L. Lyons, A. Janotti, and C. G. Van de Walle, *Phys. Rev. B* **93**, 165206 (2016).

- <sup>25</sup>S. M., M. R.H., H. M., T. D., and H. M., *physica status solidi c* **6**, 2652 (2009), <https://onlinelibrary.wiley.com/doi/pdf/10.1002/pssc.200982561>, URL <https://onlinelibrary.wiley.com/doi/abs/10.1002/pssc.200982561>.
- <sup>26</sup>C. G. V. de Walle and J. Neugebauer, *Journal of Applied Physics* **95**, 3851 (2004), <http://dx.doi.org/10.1063/1.1682673>, URL <http://dx.doi.org/10.1063/1.1682673>.
- <sup>27</sup>C. Freysoldt, B. Grabowski, T. Hickel, J. Neugebauer, G. Kresse, A. Janotti, and C. G. Van de Walle, *Rev. Mod. Phys.* **86**, 253 (2014), URL <https://link.aps.org/doi/10.1103/RevModPhys.86.253>.
- <sup>28</sup>J. P. Perdew, K. Burke, and M. Ernzerhof, *Phys. Rev. Lett.* **77**, 3865 (1996), URL <https://link.aps.org/doi/10.1103/PhysRevLett.77.3865>.
- <sup>29</sup>J. P. Perdew, K. Burke, and M. Ernzerhof, *Phys. Rev. Lett.* **78**, 1396 (1997), URL <https://link.aps.org/doi/10.1103/PhysRevLett.78.1396>.
- <sup>30</sup>J. Heyd, G. E. Scuseria, and M. Ernzerhof, *The Journal of Chemical Physics* **118**, 8207 (2003), <http://dx.doi.org/10.1063/1.1564060>, URL <http://dx.doi.org/10.1063/1.1564060>.
- <sup>31</sup>J. Heyd, G. E. Scuseria, and M. Ernzerhof, *The Journal of Chemical Physics* **124**, 219906 (2006), <http://dx.doi.org/10.1063/1.2204597>, URL <http://dx.doi.org/10.1063/1.2204597>.
- <sup>32</sup>G. Kresse and J. Furthmüller, *Phys. Rev. B* **54**, 11169 (1996), URL <https://link.aps.org/doi/10.1103/PhysRevB.54.11169>.
- <sup>33</sup>D. Colleoni and A. Pasquarello, *Phys. Rev. B* **93**, 125208 (2016).
- <sup>34</sup>P. V. C. Medeiros, S. Stafström, and J. Björk, *Phys. Rev. B* **89**, 041407 (2014), URL <https://link.aps.org/doi/10.1103/PhysRevB.89.041407>.
- <sup>35</sup>P. V. C. Medeiros, S. S. Tsirkin, S. Stafström, and J. Björk, *Phys. Rev. B* **91**, 041116 (2015), URL <https://link.aps.org/doi/10.1103/PhysRevB.91.041116>.
- <sup>36</sup>K. Momma and F. Izumi, *Journal of Applied Crystallography* **44**, 1272 (2011), URL <https://doi.org/10.1107/S0021889811038970>.
- <sup>37</sup>R. Chtourou, F. Bousbih, S. B. Bouzid, F. F. Charfi, J. C. Harmand, G. Ungaro, and L. Largeau, *Applied Physics Letters* **80**, 2075 (2002), <https://doi.org/10.1063/1.1462864>, URL <https://doi.org/10.1063/1.1462864>.
- <sup>38</sup>J. E. Lowther, S. K. Estreicher, and H. Temkin, *Applied Physics Letters* **79**, 200 (2001), <https://doi.org/10.1063/1.1383280>, URL <https://doi.org/10.1063/1.1383280>.
- <sup>39</sup>C. Kittel, *Introduction to Solid State Physics* (John Wiley & Sons, Inc., New York, 1986), 6th ed.
- <sup>40</sup>W. Shan, W. Walukiewicz, J. W. Ager, E. E. Haller, J. F. Geisz, D. J. Friedman, J. M. Olson, and S. R. Kurtz, *Phys. Rev. Lett.* **82**, 1221 (1999), URL <https://link.aps.org/doi/10.1103/PhysRevLett.82.1221>.
- <sup>41</sup>O. E. P., L. A., and F. S., *Journal of Physics: Condensed Matter* **16**, S3257 (2004), URL <http://stacks.iop.org/0953-8984/16/i=31/a=019>.
- <sup>42</sup>F. Ishikawa, S. Fuyuno, K. Higashi, M. Kondow, M. Machida, H. Oji, J.-Y. Son, A. Trampert, K. Umeno, Y. Furukawa, et al., *Applied Physics Letters* **98**, 121915 (2011), <https://doi.org/10.1063/1.3573789>, URL <https://doi.org/10.1063/1.3573789>.
- <sup>43</sup>K. M. Kim, W.-B. Kim, D. Krishnamurthy, J. H. Ryu, S. Hasegawa, and H. Asahi, *Journal of Crystal Growth* **368**, 35 (2013), ISSN 0022-0248, URL <http://www.sciencedirect.com/science/article/pii/S002202481300047X>.
- <sup>44</sup>J. Chen, G. Ciatto, M. Le Du, J.-C. Harmand, and F. Glas, *Phys. Rev. B* **82**, 125303 (2010), URL <https://link.aps.org/doi/10.1103/PhysRevB.82.125303>.
- <sup>45</sup>H. T. Pham, S. F. Yoon, K. H. Tan, and D. Boning, *Applied Physics Letters* **90**, 092115 (2007), <https://doi.org/10.1063/1.2710751>, URL <https://doi.org/10.1063/1.2710751>.
- <sup>46</sup>H. P. Nair, A. M. Crook, K. M. Yu, and S. R. Bank, *Applied Physics Letters* **100**, 021103 (2012), <https://doi.org/10.1063/1.3675618>, URL <https://doi.org/10.1063/1.3675618>.
- <sup>47</sup>J. Buckeridge, D. O. Scanlon, T. D. Veal, M. J. Ashwin, A. Walsh, and C. R. A. Catlow, *Phys. Rev. B* **89**, 014107 (2014), URL <https://link.aps.org/doi/10.1103/PhysRevB.89.014107>.